JOURNAL OF AIRCRAFT
Vol. 32, No. 3, May–June 1995

Signal Processing of Noise Data from High-Speed Flyovers

Jeffrey J. Kelly* and Mark R. Wilson†
Lockheed Engineering and Sciences Company, Inc., Hampton, Virginia 23666-1339

Narrow-band spectra characterizing jet noise are constructed from flyover acoustic measurements. Radar and c–band tracking systems provided the aircraft position histories from which directivity and smear angles from the aircraft to each microphone are computed. These angles are based on source emission time. This allowed spectra to be correlated to aircraft position at the time of sound emission. Simulated spectra are included in this article to demonstrate spectral broadening due to smear angle. A detailed description of the signal processing procedures is provided. The spectra demonstrated the forward radiation of broadband shock noise of supersonic jets, confirming what has been observed in static tests.

Nomenclature

c_0 = ambient speed of sound
f = frequency
f_k = kth bin center frequency
f_n = nth harmonic of f_0
f_R = Doppler shifted frequency
f_s = source frequency
f_0 = fundamental frequency
h = aircraft altitude
L = sound–pressure level at the observer
L_m = sound–pressure level at the source
$\boldsymbol{M}$ = aircraft Mach number vector
N = block size
N_H = number of harmonics
n_b = number of frequency bands
n_d = number of microphones
$\boldsymbol{n}_r$ = unit vector in the direction of $\boldsymbol{r}$
p_{amb} = ambient pressure
p_j = jet nozzle static pressure
$p_m(\tau)$ = time corrected pressure
r_m = reference distance
$\boldsymbol{r}_1$ = position vector between source and observer at time τ_1
T = fast Fourier transform (FFT) window duration
t = reception time
$\boldsymbol{U}$ = aircraft velocity
$\boldsymbol{x}$ = position vector
$\alpha(f)$ = absorption coefficient
Δf = frequency bin width
Δt = sampling interval, s
$\Delta\theta$ = smear angle
θ = emission angle
θ_0 = initial emission angle
θ_1 = emission angle at time τ_1
τ = emission time

Introduction

THE emphasis now placed on the high-speed civil transport (HSCT) has produced increased interest in jet noise measurements obtained from flight tests. Accurate acoustic data acquisition and signal analysis on aircraft engines that emulate the engines of the HSCT is of paramount importance.

Received Dec. 11, 1992; presented as Paper 93-0736 at the AIAA 31st Aerospace Sciences Meeting and Exhibit, Reno, NV, Jan. 11–14, 1993; revision received Oct. 20, 1994; accepted for publication Oct. 20, 1994.

*Staff Engineer, 144 Research Drive. Senior Member AIAA.
†Senior Associate Engineer, 144 Research Drive. Member AIAA.

The data presented and analyzed in this study consists of acoustic measurements on the ground for level flyovers of an F-18 aircraft. These measurements were performed at NASA Dryden Flight Research Facility, California. A linear array of 12 microphones with a spacing of 350 ft was used to acquire the data as the aircraft flew over aligned with the array. Aircraft position history, weather data (atmospheric pressure, temperature, relative humidity, etc.), and engine state parameters were also collected during the test. Position history is required for acoustic ensemble-averaging and directivity characterization. Both radar and c–band systems were employed to track the flights. Weather data is needed to determine emission time and angle. This was obtained by rawinsonde. Engine state parameters allow the jet noise source to be correlated with the observed spectra. These parameters were recorded onboard the aircraft during the flyovers. This article deals mainly with the recorded acoustic data and the construction of narrow-band source spectra characterizing jet noise.

Data Acquisition and Analysis

Flush-mounted microphones on planar ground boards were employed with a frequency response of 0.01–40,000 Hz with a maximum sound pressure level of 160 dB. The signals were FM-recorded at 15 ips, which gives a dynamic range of about 46 dB. However, before recording, the signals were bandpass-filtered from 25 Hz to 12.5 kHz to prevent aliasing and to enable accurate sound–pressure level (SPL) estimates up to the 10 kHz one-third-octave band [needed for effective perceived noise level (EPNL) calculations]. Due to the high impedance presented to the incident sound by the ground boards, a constant 6-dB frequency correction can be made for each spectral bin for reflection.

The analog data was digitized using the following Nyquist criterion:

$$\text{sample rate} = 1/\Delta t = 2.5 f_c \tag{1}$$

where f_c is the upper cutoff frequency. With $f_c = 12.5$ kHz, this yields $\Delta t = 3.2 \times 10^{-5}$ s or 31,250 samples/s. The signal was digitized and converted to engineering units (EU) by ADDRAS.[1] Each microphone channel was calibrated and the calibration signal recorded on the analog tapes prior to the flyovers.

Smear Angle and Ensemble-Averaging

At a ground-based observer, the acoustic signal from an aircraft flyover is nonstationary. Thus, the Fourier transform of the signal will be time-dependent. A short-time Fourier transform with a sliding window function[2] is the usual method

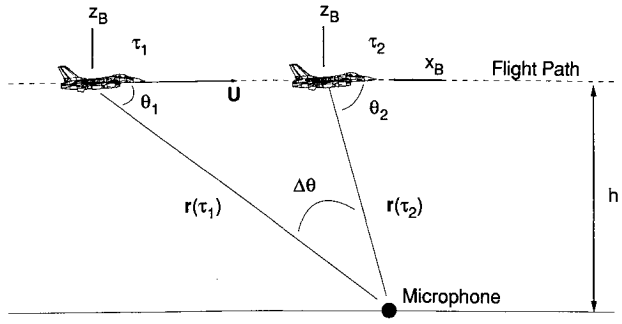

Fig. 1 Definition of emission angles.

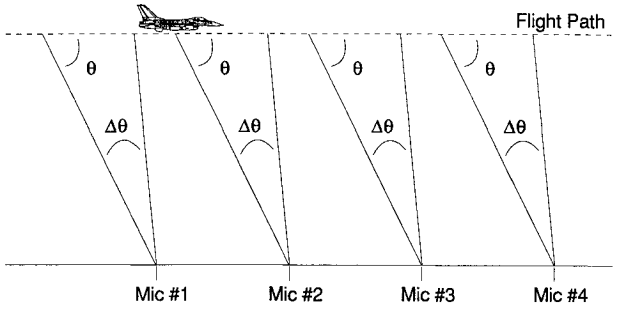

Fig. 2 Microphone configuration for ensemble-averaging.

employed to deal with this situation. A tradeoff must be made between time resolution and frequency resolution. One function of the window is to limit the duration of the time signal so that the spectral characteristics appear reasonably stationary. A rapidly varying signal requires a reduced window length. Reducing the window length reduces the frequency resolution. Increasing the window duration can lead to spectral smearing that is defined later.

To perform ensemble-averaging of acoustic flyover measurements, the averaging across a microphone array requires that each individual microphone be exposed to the same directivity angles. It will be assumed in the ensemble-averaging scheme that the aircraft is in level flight at constant velocity and a fixed orientation. Deviations from this type of flight profile can present problems to ensemble-averaging test data.

Figure 1 illustrates angles associated with smearing. The angle between $\boldsymbol{U}$ and $\boldsymbol{r}$ is denoted by θ, and is the noise emission directivity angle. The angles θ_1 and θ_2 correspond to emission times τ_1 and τ_2, respectively, associated with the fast Fourier transform (FFT) time window. The smear angle is defined as $\Delta\theta = \theta_2 - \theta_1$. Note that the angles are based on the time of signal emission and not on the time of signal reception.

As can be seen in Fig. 1, $\Delta\theta$ is a function of aircraft altitude and speed. Increasing T to improve frequency resolution (smaller bin width) is only viable if $\Delta\theta$ is small. Otherwise, severe spectral smearing, which is indicated by the broadening of spectral peaks and tones, will occur becoming more severe as $\Delta\theta$ increases. This becomes less of a problem as altitude increases or speed decreases. Smearing is more pronounced for approaching aircraft than for receding aircraft due to the upward Doppler frequency shift in conjunction with signal leakage associated with the finite time window.[3] Using a linear microphone array allows spectral-averaging across the array as shown in Fig. 2. Each microphone output is treated as an individual record in the averaging. This is possible only if each microphone measurement contains the same directivity angles that are indicated in Fig. 2.

Directivity and Smear Angle Determination

Acoustic source emission times were determined for the spectra from the radar tracking data files. Since the flight paths were approximately along the array at constant altitude, an initial emission angle corresponding to τ is designated, and a range estimate is made by the following:

$$x_s = h \cot \theta \tag{2}$$

where x_s is measured from the microphone along the array axis. The radar file is then searched to find x_s, after which τ_1 is determined by way of linear interpolation. Also, the position vector $\boldsymbol{r}(\tau)$ from the aircraft to the microphone is calculated:

$$\boldsymbol{r}(\tau) = \boldsymbol{x} - \boldsymbol{x}_s(\tau) \tag{3}$$

Here, $\boldsymbol{x}$ is the position vector of the microphone and $\boldsymbol{x}_s$ is the position vector of the aircraft obtained from the tracking history. Next, θ_1 is updated:

$$\theta_1 = \cos^{-1}(r_x/|\boldsymbol{r}|) \tag{4}$$

where r_x is the component of $\boldsymbol{r}$ along the array axis.

It is assumed in Eq. (4) that the aircraft axis is aligned parallel with the array axis. The corresponding τ is determined from the retarded time relation

$$t = \tau + [r(\tau)/c_0] \tag{5}$$

where c_0 is an averaged value of the speed of sound obtained from the rawinsonde data. The pressure–time history file is then searched to find t_1, the start time (reception time) for the FFT record. Computation of the final reception time is easily found from

$$t_2 = t_1 + T \tag{6}$$

To arrive at a smear angle $\Delta\theta$, τ_2 corresponding to t_2 must be calculated. This is done by rearranging Eq. (5) and using linear iteration[4]:

$$(\tau_2)_{l+1} = t_2 - \{r[(\tau_2)_l]/c_0\} \tag{7}$$

Here, the subscript l refers to the values of t used in the iteration. Thus, the radar file is iteratively searched until Eq. (7) converges, which determines τ_2 and $r(\tau_2)$. The convergence criterion is

$$\left|\frac{(\tau_2)_{l+1} - (\tau_2)_l}{(\tau_2)_{l+1}}\right| \leq 0.001 \tag{8}$$

Equation (4) will also yield θ_2 so that the smear angle can be computed.

Spectral Analysis

The steps used to construct the narrow-band spectra are similar to those given in Ref. 5. Equation (1) along with N determine the FFT window duration

$$T = N\Delta t \tag{9}$$

The frequency bin width is given by

$$\Delta f = 1/T \tag{10}$$

The FFT of the signal can be expressed as

$$P_i(f_k) = \Delta t \sum_{n=0}^{N-1} p_{\text{in}} \exp\left[-\frac{j2\pi kn}{N}\right] \tag{11}$$

In these relations, $P_i(f_k)$ is the output from the FFT algorithm, and the subscript i designates the particular record or micro-

phone used in the ensemble-average. The FFT subroutine employed is based on the Cooley–Tukey[6] algorithm. The discrete frequencies, which are the bin center frequencies, are given by

$$f_k = k/T, \qquad k = 0, 1, 2, \ldots, N/2 \tag{12}$$

With the FFT components computed, the power spectral density function ensemble-averaged over n_d microphones is evaluated from

$$G_{pp}(f_k) = \frac{2}{n_d T} \sum_{i=1}^{n_d} |P_i(f_k)|^2, \qquad k = 0, 1, 2, \ldots, N/2 \tag{13}$$

Using Eqs. (10) and (13), the mean-squared pressure for the bin with f_k and Δf can be approximated by

$$\overline{p^2(f_k, \Delta f)} = G_{pp}(f_k)\Delta f = \frac{2}{n_d T^2} \sum_{i=1}^{n_d} |P_i(f_k)|^2 \tag{14}$$

Thus, the sound–pressure level for the kth bin is

$$L(f_k) = 10 \log \left[\frac{\overline{p^2(f_k, \Delta f)}}{p_{\text{ref}}^2} \right] + \Delta L(f_k) \tag{15}$$

where $\Delta L(f_k)$ represents a weighting function in decibels (e.g., A weighting). If no weighting is desired then $\Delta L(f_k) = 0$. The overall sound–pressure level for a particular band is

$$L_{OA} = 10 \log \left[\sum_{k=1}^{n_b} 10^{L(f_k)/10} \right] \tag{16}$$

where n_b is the number of frequency bands employed in the level calculation. For the results presented in this study, $N = 16{,}384$ points so that $T = 0.5243$ s and $\Delta f = 1.91$ Hz. Also, $n_d = 12$ since 12 microphones were employed in the ensemble-averaging.

Spectra Simulation

An analysis of computer-simulated spectra is included to demonstrate the effects of motion. A common model for illustrating motion effects on acoustic signals is the moving point source with a pressure field described by[7]

$$p(\boldsymbol{x}, t) = \frac{p_m(\tau)}{[r(\tau)/r_m][1 - \boldsymbol{M}(\tau)\cdot\boldsymbol{n}_r(\tau)]^2} \tag{17}$$

Here, $p_m(\tau)$ has been introduced to describe the source structure in terms of pressure at r_m. In Eq. (17), τ is the time of signal emission, and t is the time of signal reception. The position vector $\boldsymbol{x}$ designates the receiver location at t. The Mach number vector $\boldsymbol{M}$ and θ correspond to τ. For subsonic motion, the Doppler amplitude factor $(1 - \boldsymbol{M}\cdot\boldsymbol{n}_r)^2$ predicts amplification of sound in the forward arc and attenuation in the rearward arc. This effect depends on both source velocity and emission angle since $(1 - \boldsymbol{M}\cdot\boldsymbol{n}_r)^2 = (1 - M\cos\theta)^2$.

A far-field approximation, assuming a small smear angle, can be derived from Eq. (17) relating observer and source narrow-band spectra:

$$\overline{p^2(f_k)} = \frac{\overline{p_m^2[f_k(1 - M\cos\theta)]}}{(r/r_m)^2(1 - M\cos\theta)^4} \tag{18}$$

Here, it is assumed that r, M, and θ are constant over the time window used in the Fourier transform. Equation (18) explicitly shows the Doppler frequency shift relation, which is expressed as

$$f_R = f_s/(1 - M\cos\theta) \tag{19}$$

Converting Eq. (18) to sound–pressure levels results in

$$L = L_m - 20\log(r/r_m) - 40\log(1 - M\cos\theta) \tag{20}$$

This expression is valid for either individual bin levels or overall levels. Equation (20) predicts a significant increase in the SPL in the forward arc of the source as the speed increases. In particular, directly in front of a source moving at $M = 0.9$, Eq. (20) shows a 40 dB increase in SPL due to motion.

In the above discussion, atmospheric absorption is ignored. Inclusion of absorption in the analysis of moving sources will alleviate the high levels implied by Eq. (20). Since absorption of sound increases with frequency and the observer spectrum is shifted to higher frequencies in the forward arc, the effects of Doppler amplification will be reduced. Adding an absorption term to Eq. (20) results in

$$L[f_s/(1 - M\cos\theta)] = L_m(f_s) - 20\log r - 40\log(1 - M\cos\theta) - 8.68\alpha[f_s/(1 - M\cos\theta)](r - 1) \tag{21}$$

In this expression, the spectral content is stated in terms of the source frequencies. For the simulated spectra presented, an absorption subroutine was chosen that is an update of the 1978 ANSI standard.[8–10] A point source in uniform motion was used to generate the pressure time series. The spectral content of the source was taken to be a summation of harmonic sinusoids and each component is attenuated by atmospheric absorption. Equation (17) is modified to account for absorption and becomes

$$p(\boldsymbol{x}, t) = \frac{\sum_{n=1}^{N_H} A_n \exp\{-\alpha[f_n/(1 - M\cos\theta)](r - 1)\}\cos[2\pi f_n \tau + (n - 1)\pi/2]}{r(\tau)[1 - \boldsymbol{M}(\tau)\cdot\boldsymbol{n}_r(\tau)]^2} \tag{22}$$

where

$$f_n = nf_0$$

Here, $f_0 = 25$ Hz is the fundamental $N_H = 100$, and each A_n corresponds to a 140-dB tone that results in a 160-dB overall sound pressure level (OASPL). The attenuation factor α is calculated from the absorption subroutine whose input is frequency, relative humidity, ambient temperature, and pressure. Using the time series generated by Eq. (22) as input to an FFT algorithm will produce a simulated spectrum at the measurement location of the moving source.

Using altitude, velocity, and θ_0 as input, the source position vector can be expressed as

$$\boldsymbol{x}_s(\tau) = x_s\boldsymbol{i} + y_s\boldsymbol{j} + z_s\boldsymbol{k} = U\tau\boldsymbol{i} \tag{23}$$

and the observer position vector as

$$\boldsymbol{x} = x\boldsymbol{i} + y\boldsymbol{j} + z\boldsymbol{k} = h\cot\theta_0\boldsymbol{i} - h\boldsymbol{j} \tag{24}$$

where $\boldsymbol{i}$, $\boldsymbol{j}$, and $\boldsymbol{k}$ are standard unit vectors. These vectors

allow the computation of $r(\tau)$ by means of Eq. (3). Also, Eq. (5) can be solved explicitly for τ in terms of t

$$\tau = \frac{c_0 t - Mx - \sqrt{(x - Ut)^2 + (1 - M^2)^2 y^2}}{c_0(1 - M^2)} \quad (25)$$

Equation (25) is needed for signal processing based on reception time since FFT algorithms require equally spaced samples.

Three flight profiles similar to those obtained in the F-18 flight test were chosen to construct the simulated signals. They were all at an altitude of 1500 ft with $M = 0.3$, 0.6, and 0.95. Atmospheric parameters employed were averaged values obtained from the Dryden rawinsonde data. Signal processing parameters used to construct the spectra are $\Delta t = 4 \times 10^{-5}$ s, $N = 16{,}384$ points, $T = 0.655$ s, and $\Delta f = 1.5$ Hz.

Figure 3 shows the computed source spectrum (without motion). The variation in the spectral peaks is due to leakage caused by using a rectangular time window in the FFT. Spectra are displayed in Figs. 4–9 for two initial emission angles, $\theta_1 = 45$ deg (forward radiation) and 135 deg (aft radiation), for each Mach number. These angles were chosen to demonstrate the effects of smear angle for both approaching and receding

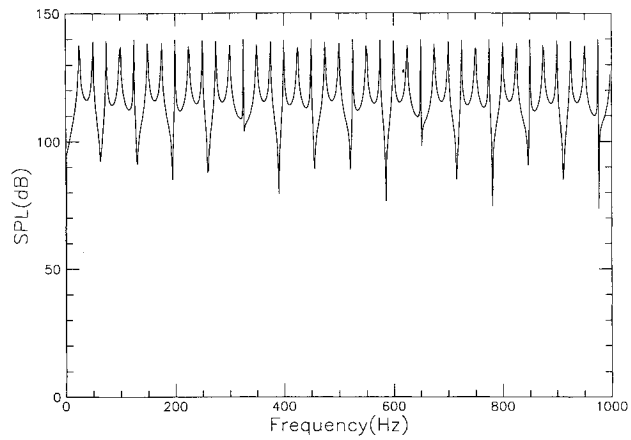

Fig. 3 Stationary simulated source spectrum.

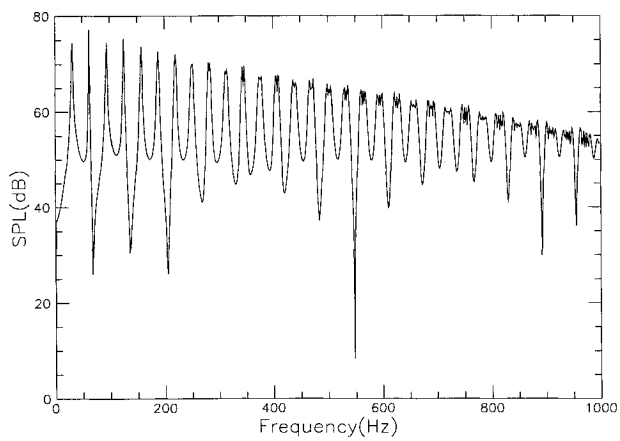

Fig. 4 Moving simulated spectrum, $M = 0.3$, $\theta_1 = 45$ deg, $\Delta\theta = 5.68$ deg.

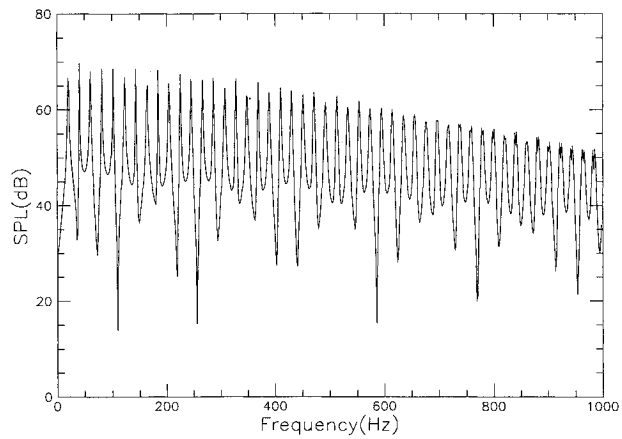

Fig. 5 Moving simulated spectrum, $M = 0.3$, $\theta_1 = 135$ deg, $\Delta\theta = 3.2$ deg.

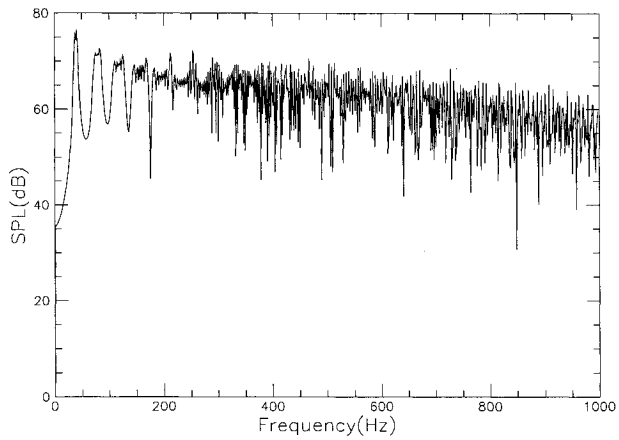

Fig. 6 Moving simulated spectrum, $M = 0.6$, $\theta_1 = 45$ deg, $\Delta\theta = 16.37$ deg.

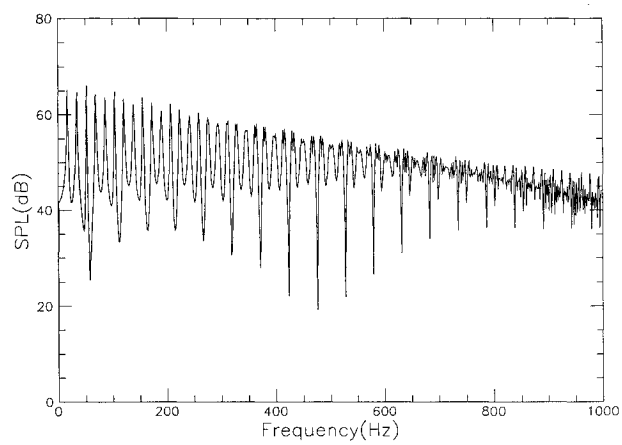

Fig. 7 Moving simulated spectrum, $M = 0.6$, $\theta_1 = 135$ deg, $\Delta\theta = 5.18$ deg.

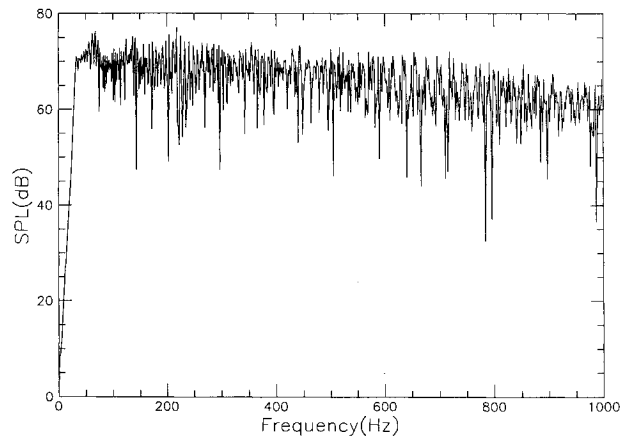

Fig. 8 Moving simulated spectrum, $M = 0.95$, $\theta_1 = 45$ deg, $\Delta\theta = 35.9$ deg.

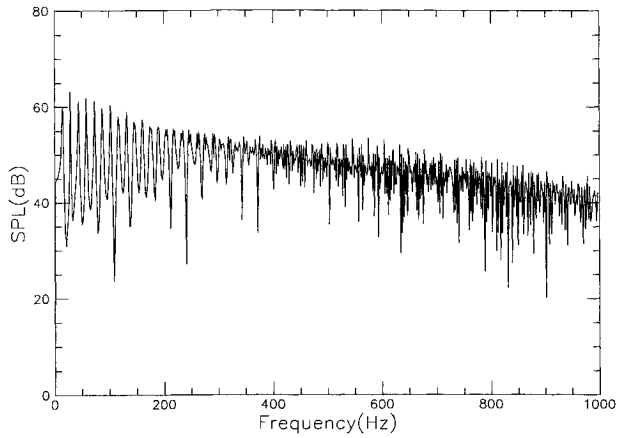

Fig. 9 Moving simulated spectrum, $M = 0.95$, $\theta_1 = 135$ deg, $\Delta\theta = 6.7$ deg.

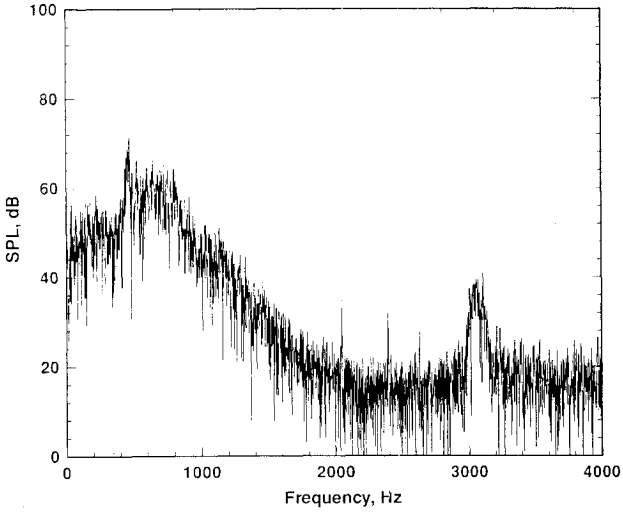

Fig. 10 F-18 spectrum for a single microphone, $M = 0.3$, $\theta_1 = 14.95$ deg, $\Delta\theta = 0.95$ deg.

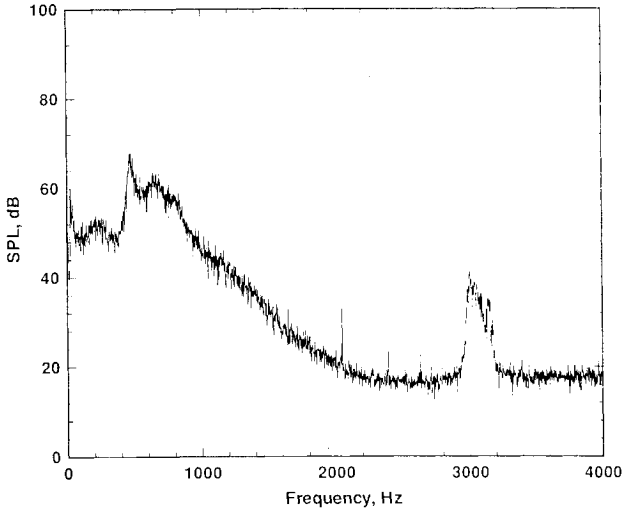

Fig. 11 F-18 ensemble-averaged spectrum, $M = 0.3$, $\theta_1 = 15$ deg, $\Delta\theta = 0.99$ deg.

segments of the flight path. Smear angle affects the spectra by broadening the spectral peaks so that they appear as broadband noise. The severity of spectral smearing increases with frequency and smear angle as shown in the figures. For Fig. 4, the effect of smearing first becomes significant in the vicinity of 300 Hz. In contrast it is not discernible below approximately 750 Hz in Fig. 5. Increasing the Mach number to $M = 0.6$ results in the spectra depicted in Figs. 6 and 7

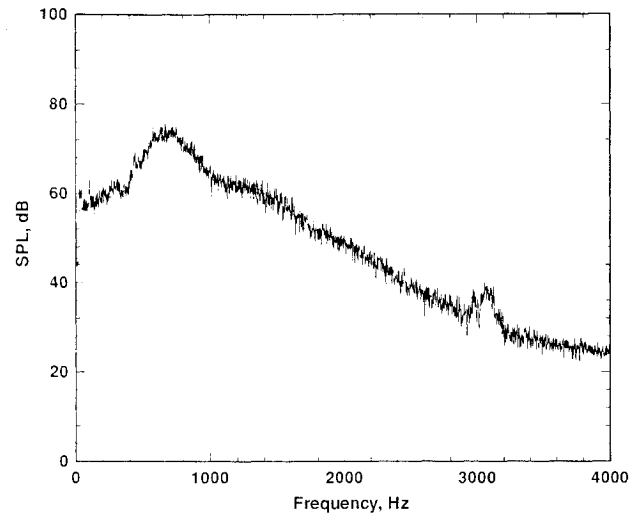

Fig. 12 F-18 ensemble-averaged spectrum, $M = 0.3$, $\theta_1 = 35.15$ deg, $\Delta\theta = 5.03$ deg.

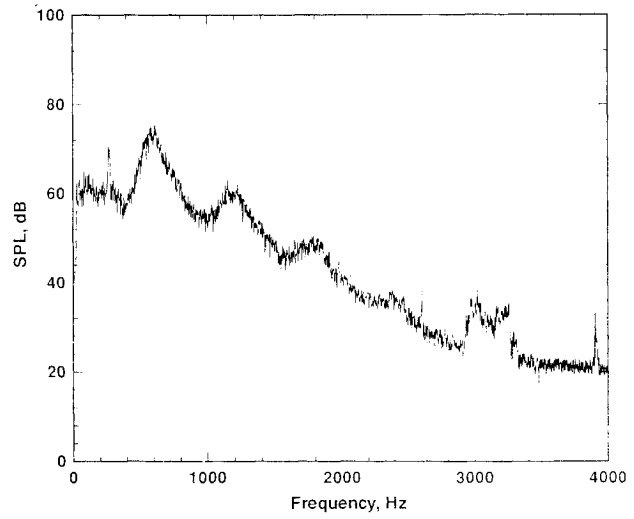

Fig. 13 F-18 ensemble-averaged spectrum, $M = 0.8$, $\theta_1 = 15.63$ deg, $\Delta\theta = 5.32$ deg.

where spectral smearing now occurs throughout the spectrum for $\theta_1 = 45$ deg, and at around 350 Hz and above for $\theta_1 = 135$ deg. Figures 8 and 9 illustrate what happens for $M = 0.95$. In Fig. 8, $\theta_1 = 45$ deg, tones are not perceptible throughout the spectrum due to the resulting large smear angle $\Delta\theta = 35.9$ deg. Figure 9 shows that tones are apparent below 300 Hz for $\theta_1 = 135$ deg since this spectrum contains a reduced smear angle of $\Delta\theta = 6.7$ deg.

Application of Developed Techniques to Real Flight Data

Figures 10–12 contain spectra that were constructed from F-18 acoustic measurements with one engine at flight idle at an altitude of 1500 ft and Mach number of 0.3. To demonstrate the effects of ensemble-averaging across the array, the spectrum from a single microphone is shown in Fig. 10. Figure 11 shows the results of acoustic ensemble-averaging over 12 microphones for the same flyover. Although there is only a small difference between the overall SPLs in the two figures, the smoothing effect of averaging is clearly seen. Characteristics of broadband shock-associated noise are more discernible[11,12] in Fig. 11. It shows the presence of spectral peaks at 450 and 650 Hz due to shock noise. The spectral peak in the vicinity of 3 kHz is internal noise generated by the data acquisition system. Spikes at harmonics of 60 Hz, such as 2.04 and 2.4 kHz in Fig. 11 can be attributed to the power generator that

was the electrical supply to the instrumentation van. Since $p_j/p_{amb} = 0.51$, meaning that the jet is overexpanded, shocks are present. Figure 12 shows the spectrum for $\theta_1 = 35.15$ deg, and thus contains a larger smear angle, $\Delta\theta = 5.03$ deg. A single peak is visible centered at about 700 Hz. Compared to static data, flight test spectra will contain spectral smearing that can become quite significant with increased source velocity and for higher frequencies. Thus, any tonal structure will appear broadened to a ground observer, especially in the forward arc of the aircraft acoustic field.

Figure 13 displays an F-18 flyover ensemble-averaged spectrum for $M = 0.8$, where $\theta_1 = 15.63$ deg. Again, features of broadband shock noise are apparent. Notice that there are spectral peaks centered at 600 Hz, 1.2 kHz, and 1.8 kHz. These measured spectra displayed in this article and additional spectra not shown illustrated that broadband-shock noise radiates forward of the nozzle, which has been observed in static tests.[11]

Summary

Narrow-band acoustic spectra were constructed from aircraft flyover measurements in which jet noise was the dominant source. Aircraft position history was also acquired during the data collection. A numerical scheme was devised in order to determine directivity angles from the aircraft to each microphone based on source emission time. This allowed spectra to be correlated to aircraft position at the time of sound emission. Also, smear and emission angles based on emission time are calculated for each spectrum. A detailed description of the signal processing procedures and concerns for measuring jet noise is included in the study. Some results from a simulation model are presented in this article, which demonstrate spectral smearing due to source motion. The results of the spectral constructions from the flight-test data show features signifying broadband-shock noise and its highly directional nature, confirming what has been observed in static tests.

Acknowledgment

This study was supported by NASA Langley Research Center Contract NAS1-19000.

References

[1]Becker, L. E., Rutledge, C. K., Grandle, R. E., Golub, R. A., and Smith, R. A., "ADDRAS—An Integrated Systems Approach," American Helicopter Society/Royal Aeronautical Society International Technical Specialists Meeting, Rotorcraft Acoustics and Rotor Fluid Dynamics, Philadelphia, PA, Oct. 1991.

[2]Oppenheim, A. V., and Schafer, R. W., *Discrete-Time Signal Processing*, Prentice–Hall, Englewood Cliffs, NJ, 1989, pp. 713–716.

[3]Kelly, J. J., "Signal Processing of Aircraft Flyover Noise," NASA CR 187546, May 1991.

[4]Henrici, P. K., *Elements of Numerical Analysis*, Wiley, New York, 1964.

[5]Bendat, J. S., and Piersol, A. G., *Random Data: Analysis and Measurement Procedures*, Wiley-Interscience, New York, 1986, pp. 391–393.

[6]Cooly, J. W., and Tukey, J. W., "An Algorithm for the Machine Calculation of Complex Fourier Series," *Mathematics of Computation*, Vol. 19, April 1965, p. 297.

[7]Dowling, A. P., and Ffowcs-Williams, J. E., *Sound and Sources of Sound*, Ellis Horwood, Chichester, England, UK, 1983, Chap. 9.

[8]ANSI S1.26-1978, "American National Standard Method for the Calculation of the Absorption of Sound by the Atmosphere," American National Standards Inst., New York, 1978.

[9]Zuckerwar, A. J., and Meredith, R. W., "Low-Frequency Absorption of Sound in Air," *Journal of the Acoustical Society of America*, Vol. 78, No. 3, 1985, pp. 946–955.

[10]Bass, H. E., Sutherland, L. C., and Zuckerwar, A. J., "Atmospheric Absorption of Sound: Update," *Journal of the Acoustical Society of America*, Vol. 88, No. 4, 1990, pp. 2019–2021.

[11]Norum, T. D., and Seiner, J. M., "Measurements of Mean Static Pressure and Far Field Acoustics of Shock-Containing Supersonic Jets," NASA TM-84521, Sept. 1982.

[12]Tam, C. K. W., "Broadband Shock Associated Noise of Supersonic Jets Measured by a Ground Observer," AIAA Paper 92-0502, Jan. 1992.